



HAL
open science

Nonlinear optical properties of Rh-Pd and Rh-Pt solid-solution alloy nanoparticles prepared by a laser-induced nucleation method in aqueous solution

Islam Sarker, Takahiro Nakamura, Ali Hossain, Yuichi Kozawa, Shunichi Sato

► **To cite this version:**

Islam Sarker, Takahiro Nakamura, Ali Hossain, Yuichi Kozawa, Shunichi Sato. Nonlinear optical properties of Rh-Pd and Rh-Pt solid-solution alloy nanoparticles prepared by a laser-induced nucleation method in aqueous solution. *OSA Continuum*, 2019, 2 (10), pp.2891-2900. 10.1364/OSAC.2.002891 . hal-02366447

HAL Id: hal-02366447

<https://amu.hal.science/hal-02366447>

Submitted on 15 Nov 2019

HAL is a multi-disciplinary open access archive for the deposit and dissemination of scientific research documents, whether they are published or not. The documents may come from teaching and research institutions in France or abroad, or from public or private research centers.

L'archive ouverte pluridisciplinaire **HAL**, est destinée au dépôt et à la diffusion de documents scientifiques de niveau recherche, publiés ou non, émanant des établissements d'enseignement et de recherche français ou étrangers, des laboratoires publics ou privés.



Distributed under a Creative Commons Attribution 4.0 International License

Nonlinear optical properties of Rh–Pd and Rh–Pt solid-solution alloy nanoparticles prepared by a laser-induced nucleation method in aqueous solution

MD. SAMIUL ISLAM SARKER,^{1,*}  TAKAHIRO NAKAMURA,² ALI HOSSAIN,¹ YUICHI KOZAWA,²  AND SHUNICHI SATO²

¹Department of Physics, University of Rajshahi, Rajshahi-6205, Bangladesh

²Institute of Multidisciplinary Research for Advanced Materials, Tohoku University, Katahira 2-1-1, Aoba-ku, Sendai 980-8577, Japan

*samiul-phy@ru.ac.bd

Abstract: The nonlinear optical properties of Rh–Pd and Rh–Pt solid-solution alloy nanoparticles (NPs) were experimentally investigated by means of the *z*-scan technique. The open aperture (OA) measurement showed a reverse saturable behavior, whereas the closed aperture (CA) measurement showed a peak- and valley-shape. Both the Rh–Pd and Rh–Pt NPs exhibited a positive nonlinear optical index of refraction at 800 nm relating to the self-focusing phenomenon. In addition, the nonlinear absorption of the Rh–Pt NPs (4.39×10^{-12} cm/W) was higher than that of the Rh–Pd NPs (1.63×10^{-12} cm/W) due to the small interval between the occupied and unoccupied density of states (DOS) of Rh–Pt than Rh–Pd. The nonlinear responses of the Rh–Pd and Rh–Pt NPs was attributed to the hot electron contribution and the reverse saturation of intraband and interband transitions.

© 2019 Optical Society of America under the terms of the [OSA Open Access Publishing Agreement](#)

1. Introduction

Due to the advanced technique for the preparation of nanoparticles (NPs) with well controlled size, structure and composition, it is possible to extend the study on nonlinear optical properties from organic materials to NPs based systems. The nonlinear optical properties of noble metal NPs such as Au, Ag, Cu, Pt, and Pd possess surface plasmon resonance (SPR) bands in the UV-visible range have been extensively studied [1–5]. The nonlinear optical properties of metallic NPs are important for several applications such as optical limiters, optical data storage and optical switching [4,5–8]. Optical nonlinearities such as saturable absorption (SA) and reverse saturable absorption (RSA) have been reported in different nanomaterials. Saturation of excited state or bleaching of ground state results in SA, while, free carrier absorption (FCA) or multiphoton absorption causes the RSA [9–16]. Materials exhibiting SA are used for optical pulse compression, optical switching and laser pulse narrowing. On the other hand, materials exhibiting RSA used for optical limiters in eye protections and sensors against the damage of sudden light exposure with high intensity, and it still remains a challenging problem.

Transition metal NPs, especially the Rh, Pd and Pt NPs and their alloys have attracted intensive interests for their catalytic activities [17–21]. However, quite a few researches have been reported for their nonlinear optical properties. For example, G. Fang et al. [4] reported the nonlinear absorption and refraction of Pd NPs using the *z*-scan technique. They used a nanosecond laser at a wavelength of 532 nm and revealed that the nonlinear optical absorption of Pd NPs was attributed to SA and two photon absorption (TPA). Moreover, Ganeev et al. [22] also reported the nonlinear optical properties of Au, Pd, Pt and Ru NPs using the *z*-scan technique with different pulse durations at 792 nm. They have reported a self-focusing effect of Pd NPs. When the sample was pumped by 120 fs pulse, positive nonlinear absorption was found over a broad range

of pulse intensity variations, and it became negligible when the sample was pumped by 210 ps pulse. Ganeev et al. [23] had also investigated the nonlinear absorption and refraction of Ru, Pd, and Au NPs using the z-scan technique with 50 ps laser pulses at 1064 nm and found that the Pd NPs exhibited a self-defocusing effect and positive nonlinear absorption. They predicted the nonlinear refraction arises from the optical Kerr effect. Besides, G. Fang et al. [5] also studied the nonlinear absorption and refraction of Pd and Pt NPs using femtosecond pulses and explained the nonlinear absorption was due to the TPA. However, to our best knowledge, optical nonlinearities of nanometer-sized Rh–Pd and Rh–Pt alloy particles have not yet been investigated because of the difficulties in the formation of these particles.

We had demonstrated the formation of solid-solution alloy NPs with tunable compositions by laser-induced nucleation method. In the method, alloy NPs were easily formed by high-intensity femtosecond irradiation of metallic ion solutions with different mixing ratios [24–26]. The main objective of this research is to study the third order nonlinear optical properties of Rh–Pd and Rh–Pt NPs synthesized through the laser-induced nucleation method. The nonlinear optical properties of around 10 nm-sized Rh–Pd, Rh–Pt NPs were measured using a single beam z-scan technique using a femtosecond laser. The measurements were carried out for both an open- and closed-aperture z-scan setup. The mechanism of nonlinearity has been discussed in detail.

2. Experimental details

In order to perform z-scan measurement, colloidal dispersions of Rh–Pd and Rh–Pt NPs were prepared as follows. Initially, Rh, Pd, Pt aqueous solutions were prepared separately by dissolving powders of $\text{RhCl}_3 \cdot 3\text{H}_2\text{O}$ (99.5%, Wako pure chemical industries Ltd.), PdCl_2 and $\text{H}_2\text{PtCl}_6 \cdot 6\text{H}_2\text{O}$ (99.9%, Sigma Aldrich) in ultra-pure water with the concentration of 2.5×10^{-4} M. The aqueous solution containing Rh, Pd and Pt ions were then mixed with 1 : 1 molar ratio of Rh–Pd and Rh–Pt. In order to protect particles from aggregation, 7 wt% citrate was used as a stabilizing agent. Following the preparation of the solution, 3 ml of the as-prepared solution was exposed to femtosecond laser pulses with a wavelength of 800 nm and a pulse duration of 100 fs (Spitfire Pro, Spectra Physics). Irradiation time was set for 30 min. The details of the synthesis procedure have been reported elsewhere [24]. Size and shape of fabricated particles were obtained by a transmission electron microscope (TEM; JEOL, JEM2000EXII) observation operated at 200 kV. The crystalline structures of fabricated particles were determined by powder X-ray diffraction (XRD, RINT-V, Rigaku Co.) with a Ni-filtered $\text{Cu } K_\alpha$ ($\lambda = 0.15406$ nm) X-ray source.

The nonlinear optical properties of the samples were characterized by the z-scan technique [27]. In the experiment, a Ti:sapphire ($\lambda = 800$ nm) laser with a pulse duration of 100 fs was applied at a pulse repetition rate of 100 Hz. The intensity profile of the laser beam was confirmed to be a Gaussian distribution. The experimental setup for the z-scan measurement is shown in Fig. 1. Initially, a glass cuvette of 1 mm thickness was filled with colloidal solution of alloy NPs and placed on a uniaxial stage. A collimated Ti:sapphire laser beam was focused by a lens with a focal length of 400 mm. A sample was then moved along the beam axis around the focal area to observe the change in intensity of the transmitted beam. The waist of the focused beam ($1/e^2$ width) was estimated to be 40.7 μm . The Rayleigh range of the beam was calculated to be 13 mm following the equation $z_o = 0.5 k \omega_o^2$, where $k = 2\pi/\lambda$ is the wavenumber, and $2\omega_o$ is the beam waist. The calculated intensity at the focus was 2.02×10^{12} W/cm^2 . The laser pulse energy was measured by an energy meter. In OA system, a photodiode had a sufficiently broad aperture was placed far from the focus so that the transmitted radiation was entirely detected. The sample was then moved along the beam axis and the light power transmitted through the sample was recorded. By contrast, the light power for CA was measured after passing through an aperture. The radiation energy recorded by the photodiode in the far field was normalized to the radiation energy recorded before focusing in order to avoid the influence of instability of laser parameters.

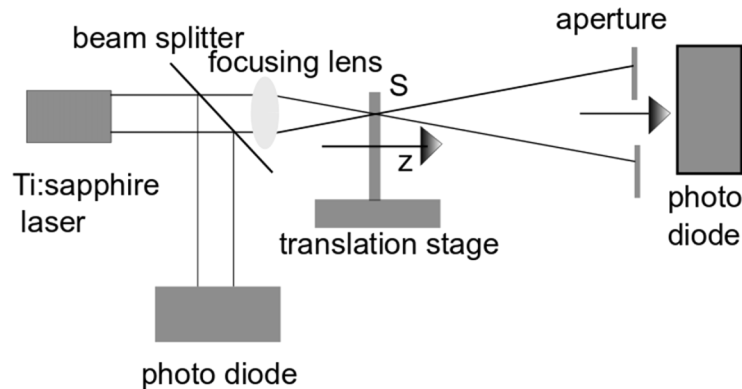


Fig. 1. Experimental setup for the measurement of nonlinear optical characteristics of NPs suspension through a z-scan technique.

3. Results and discussions

3.1. Characterization of Rh–Pd and Rh–Pt NPs

To confirm the characteristics and structures of the Rh–Pd and Rh–Pt NPs, UV-visible spectroscopy and TEM analysis was performed. Figure 2 shows the UV-visible absorption spectra of colloidal solutions and TEM images of Rh–Pd and Rh–Pt samples. It is seen from UV-visible spectra that the SPR peaks of Rh–Pd and Rh–Pt are at 270 and 250 nm, respectively. The average size of the NPs measured from TEM images were 10.2 ± 2.3 and 11.8 ± 3.3 nm for Rh–Pd and Rh–Pt systems, respectively. Further structural analysis of alloy NPs was performed through HAADF-STEM (high angle annular dark field scanning TEM) and STEM-EDX (scanning TEM energy dispersive X-ray spectroscopy) elemental mapping of samples as shown in Fig. 3. Elemental distribution of Rh–Pd and Rh–Pt alloy NPs were analyzed and shown in Fig. 3(b) and (d). It was clearly illustrated in the figure that each element was homogeneously distributed in the particles. There is no evidence for the formation of core-shell structured or phase-segregated particles.

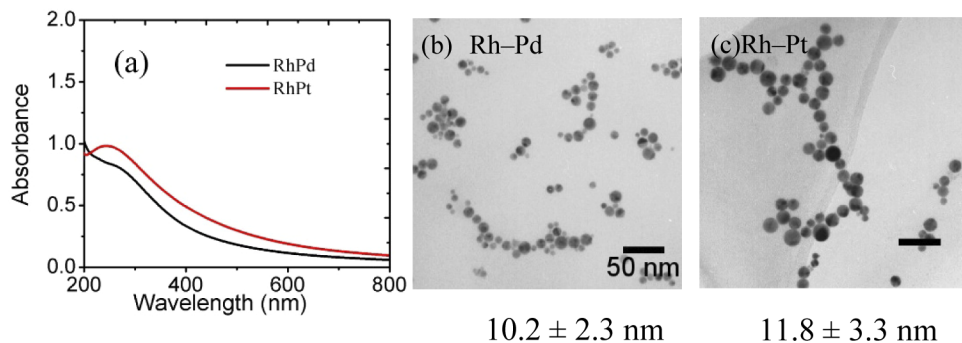


Fig. 2. (a) UV-vis spectra of colloidal suspensions and TEM images of (b) Rh–Pd and (c) Rh–Pt NPs.

Further, XRD measurement was performed for Rh–Pd and Rh–Pt system to confirm the crystalline structure and compositions of bimetallic NPs. Figure 4 shows XRD profiles for the particles fabricated in the 1: 1 ratio of Rh–Pd and Rh–Pt solution of metal ions. The vertical dot, dash-dot and solid lines indicate the peak positions for (111) and (200) planes of Rh, Pd, and Pt. A single peak was detected from each sample in the measurement angle range. The

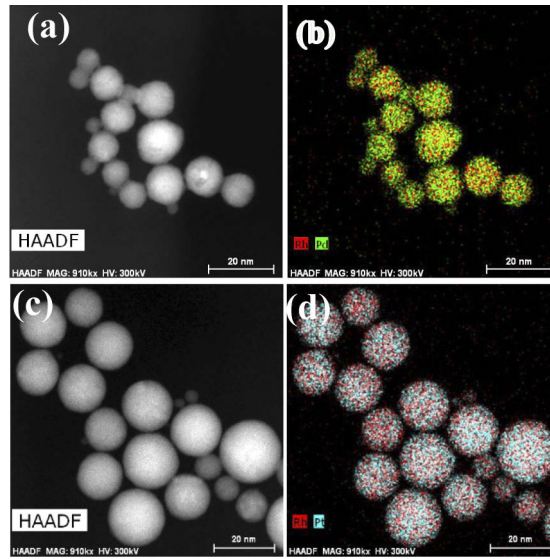


Fig. 3. (a), (c) represents HAADF-STEM images and (b), (d) shows the corresponding EDX mappings of Rh–Pd and Rh–Pt NPs synthesized by laser-induced nucleation.

XRD peak positions of Rh–Pd and Rh–Pt NPs for (111) and (200) peak reflections were located among the peaks of pure Rh, Pd and Pt indicates homogeneous alloy formation occurs through interdiffusion of Rh and Pd as well as for the Rh–Pt system. This observation strongly indicates that the fabricated alloys NPs are solid solution. The crystalline size of NPs calculated from Scherrer's equation for full width at half maximum (FWHM) of (111) reflections are 11.5 nm and 12.3 nm, respectively for Rh–Pd and Rh–Pt system, which is well matched with values measured by TEM observation.

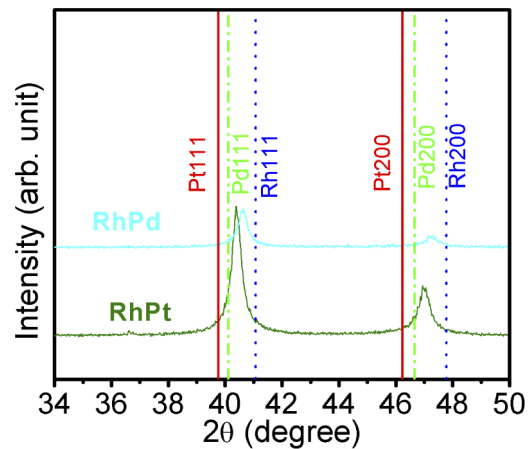


Fig. 4. XRD patterns of NPs in the mixed solutions of Rh, Pd and Pt ions.

The lattice parameter for alloy NPs was estimated from interplanar spacing of fcc structure as follows:

$$\frac{1}{d_{hkl}^2} = \frac{1}{a^2}(h^2 + k^2 + l^2)$$

here a is the lattice parameter and (hkl) is the given lattice plane. The calculated value of lattice parameters of the fabricated NPs for Rh–Pd and Rh–Pt are 3.846 Å and 3.867 Å, respectively. The lattice parameters obtained from diffraction peaks of (111) plane for Rh–Pd and Rh–Pt lies in the range of pure Rh ($a = 3.797$ Å), Pd (3.889 Å), and Pt (3.918 Å) [24]

3.2. Nonlinear absorption of Rh–Pd and, Rh–Pt alloy NPs

To confirm the measurement of nonlinear absorption, the as-synthesized Rh–Pd and Rh–Pt colloids were filled in a glass cell with an inner optical path length of 1 mm and the OA z-scan experiments were performed using 800 nm laser pulses (Fig. 1). Figure 5 shows the normalized transmittance as a function of position of the sample in the open aperture z-scan experiment for the peak intensity at the focus of 1.08×10^{12} W cm⁻². The obtained curves for (a) Rh–Pd and (b) Rh–Pt NPs indicated that when the sample was far from the focal point of the lens the laser radiation intensity was low and the normalized transmission was close to unity. On the other hand, as the sample was moved closer to the focal point, the transmission decreased monotonically and reached a minimum at the focal point. The presence of a minimum in OA z-scan curves for Rh–Pd and Rh–Pt NPs revealed the existence of the RSA. The above-mentioned phenomenon is mainly caused by so-called TPA [4]. The origin of TPA can be explained as follows. For metal NPs, only the electrons with the energy close to the Fermi level can absorb the photons of visible and near infrared light [4]. For both interband and intraband transitions, when an electron in the ground state absorbs two photons simultaneously and is excited to an upper state, this process is called TPA and leads to RSA. In contrast, an electron in the ground state absorbs one photon, which is called single photon absorption and leads to SA. According to the spectrum in Fig. 2(a), the wavelength of the used laser lies in the non-resonant regime for both of Rh–Pd and Rh–Pt alloy NPs. Therefore, the local field enhancement was not due to the SPR wavelength. Ganeev et al. [20] performed a z-scan experiment of Pd NPs with 120 fs and 210 ps laser pulses at the wavelength of 792 nm, however, they did not find SA even if the irradiation intensity is sufficiently low. A succeeding experiment with 28 ns pulse at a wavelength of 532 nm resulted in a similar conclusion [28].

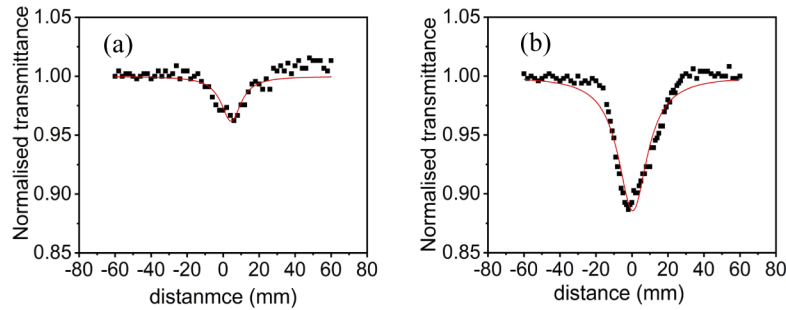


Fig. 5. OA z-scan experimental (closed circles) data and theoretical fittings (solid lines) of (a) Rh–Pd and (b) Rh–Pt NPs.

The normalized transmittance, $T(z)$, for OA z-scan experiment can be expressed by [27]

$$T(z) = \sum_{m=0}^{\infty} \frac{[-q_0(z, 0)]^m}{(m+1)^{3/2}}, \quad (1)$$

where, q_0 is defined as $q_0(z, 0) = \beta I_0 L_{eff} / (1 + z^2 / z_0^2)$, $I_0 = 2P_{in} / \pi \omega_0^2$ is the peak intensity at the focus of z-scan experiment and L_{eff} is the effective thickness of the sample deduced by $L_{eff} = (1 - e^{-\alpha_0 L}) / \alpha_0$, where, L is the sample length, z is the position of a sample and z_0 is

the Rayleigh length of the beam. The nonlinear absorption coefficient β is obtained by fitting the experimental data with Eq. (1). In Fig. 5, the dotted and solid lines were the normalized transmittance and the theoretical fitting of the experimental curve, respectively. As a result, the nonlinear absorption coefficients for Rh-Pd and Rh-Pt were obtained to be $1.63 \times 10^{-12} \text{ mW}^{-1}$ and $4.39 \times 10^{-12} \text{ mW}^{-1}$, respectively.

3.3. Nonlinear refraction of Rh-Pd and, Rh-Pt alloy NPs

The CA normalized transmittance of Rh-Pd and Rh-Pt NPs are shown in Fig. 6. The peak intensity at the focus of the CA z-scan was $1.08 \times 10^{12} \text{ Wcm}^{-2}$ for both the Rh-Pd and Rh-Pt NPs.

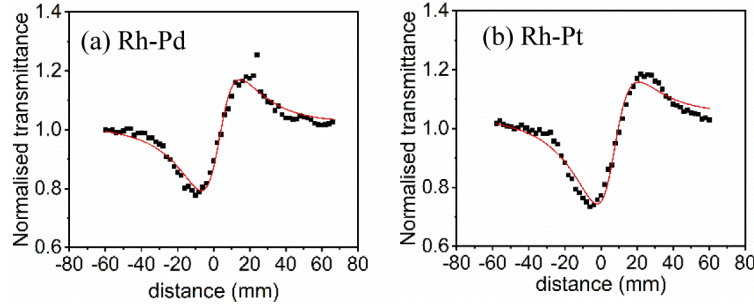


Fig. 6. Experimental data (closed circles) and theoretical fits (solid lines) for CA scheme of the colloidal suspensions of (a) Rh-Pd and (b) Rh-Pt NPs synthesized through laser-induced nucleation method.

It was reported that a prefocal transmittance maximum (peak) followed by a postfocal transmittance minimum (valley) is the signature of negative nonlinear refraction. In contrast, an opposite valley-peak configuration is attributed to positive nonlinear refraction [27]. Hence, the valley to peak shape observed in Fig. 6 indicates that the Rh-Pd and Rh-Pt NPs possess positive nonlinear refraction at 800 nm. To calculate a nonlinear refractive index, the normalized transmittance for the CA z-scan experiment $T(z)$ was fitted to the following equation [29],

$$T(z) = 1 + \frac{4x}{(x^2 + 9)(x^2 + 1)} \Delta\Phi - \frac{4(x^2 + 3)}{(x^2 + 9)(x^2 + 1)} \Delta\Psi, \quad (2)$$

where $x = z/z_0$ is the relative position from the beam waist, and $\Delta\Phi$ and $\Delta\Psi$ are the nonlinear phase shifts due to nonlinear refraction and absorption related with

$$\Delta\Phi = k\gamma I_0 L_{eff}, \quad (3)$$

$$\Delta\Psi = \beta I_0 L_{eff} / 2. \quad (4)$$

In Eqs. (3) and (4), I_0 is the peak intensity at focus and L_{eff} is the effective thickness of the sample as formulated in the OA technique. By introducing the relation $\rho = \beta/2k\gamma$, we can get the relation between $\Delta\Phi$ and $\Delta\Psi$ from Eqs. (3) and (4) as follows,

$$\Delta\Psi = \rho \Delta\Phi. \quad (5)$$

In that case, Eq. (2) can be written as

$$T(z) = 1 + \frac{2(-\rho x^2 + 2x - 3\rho)}{(x^2 + 9)(x^2 + 1)} \Delta\Phi. \quad (6)$$

The nonlinear refractive index (γ) of the samples was obtained by fitting the normalized transmittances to Eq. (6). The solid curves in Fig. 6 are the best theoretical fits to the experimental

data. The values of nonlinear refractive index are tabulated in Table 1. It is seen that the value of γ for Rh–Pd and Rh–Pt are 1.10×10^{-16} and $1.17 \times 10^{-16} \text{ cm}^2\text{W}^{-1}$, respectively. The positive values indicate the self-focusing arising from the Kerr effect of the Rh–Pd and Rh–Pt NPs. Ganeev et al. also reported positive nonlinearity of the Pd NPs using 120 fs pulse [22]. However, G. Fan et al. reported negative nonlinearity of the Pd NPs using 4 ns pulse [4].

Table 1. Nonlinear optical parameters measured at 800 nm of colloidal suspension of Rh–Pd and Rh–Pt NPs.

Estimated parameters	Sample	
	Rh–Pd	Rh–Pt
β (10^{-12} cm/W)	1.63	4.39
γ ($10^{-16} \text{ cm}^2\text{W}^{-1}$)	1.10	1.17
$\text{Re}\chi^{(3)}$ (10^{-12} esu)	1.51	1.61
$\text{Im}\chi^{(3)}$ (10^{-11} esu)	1.43	3.85
$\chi^{(3)}$ (10^{-11} esu)	1.44	3.85

The absolute value of third order nonlinear refractive index is calculated by [30]

$$|\chi^{(3)}| = [(\text{Re } \chi^{(3)})^2 + (\text{Im } \chi^{(3)})^2]^{1/2}, \quad (7)$$

where $\text{Re } \chi^{(3)}(\text{esu}) = 10^{-4} \frac{\epsilon_0 c^2 n_0^2}{\pi} \gamma c \chi_r^{(3)}$ ($\text{cm}^2 \text{ W}^{-1}$), $\text{Im} \chi^{(3)}(\text{esu}) = 10^{-2} \frac{\epsilon_0 c^2 n_0^2 \lambda}{4\pi^2} \beta$ ($\text{cm}^2 \text{ W}^{-1}$), c is the velocity of light in vacuum and ϵ_0 is the vacuum permittivity. The values of third order nonlinear susceptibility are shown in Table 1.

The values of $\chi^{(3)}$ are 1.44×10^{-11} and 3.85×10^{-11} esu for the Rh–Pd NPs and Rh–Pt NPs, respectively. $\chi^{(3)}$ of the Rh–Pt NPs is larger than that of the Rh–Pd NPs. Moreover, it is also larger than the Pt nonlinear susceptibility reported for Nd: YAG laser at a wavelength of 1064 nm [28], which can be attributed to the creation of hot electrons excited by femtosecond laser pulse [31].

The metal NPs were have been known to exhibit strong nonlinear response due to the surface plasmon resonance (SPR), which enhanced the local electric field near the NPs [32–36]. However, for the Rh–Pd and Rh–Pt alloy NPs, the SPR peaks were respectively observed at 270 nm and 250 nm (Fig. 2), which were close to 330, 225 and 215 nm for pure Rh, Pd and Pt NPs, respectively [37–39]. Because the wavelength of the laser (800 nm) is far from the SPR wavelengths, the contribution of SPR to the nonlinear response of the Rh–Pd and Rh–Pt NPs would be negligible.

The optical properties of noble metals such as Rh, Pd and Pt are influenced by the localized outermost electrons in the d band and the quasi-free-electrons in the s – p conduction band. The d band lies in the range of 2.0 to 5.0 eV below the Fermi level and is flat for almost all wave vectors \mathbf{k} [40]. Because of their relatively large effective mass, the d electrons are weakly affected by the confining potential resulting in marginal contribution to the optical transition probability. In contrast, the s – p band is extremely uneven in the k space and the effective mass of an electron is very close to that of a free electron [40]. According to the band structures of Rh, Pd and Pt, the transition can only take place around the L point of the Brillouin zone [41], which includes the intraband transition in the conduction band and the interband transition between the d band and the conduction band. The energy band structures of Rh, Pt and Pd are similar with each other [42]. Anderson has studied the energy band structures of Rh, Pt and Pd around the L point of the Brillouin zone. He found that the d bandwidth of Pd was smaller than those of Rh and Pt and the insertion of s – p band into d band for Rh and Pt is stronger than Pd [43]. Therefore, around the L point of the Brillouin zone, the interval between d band and s – p band of Rh–Pt NPs is presumed to be smaller than that of Rh–Pd NPs. Accordingly, it can be expected that the interval between occupied and unoccupied DOS curves of Rh–Pt NPs is also smaller than that of Rh–Pd

NPs. This is because that the value of occupied and unoccupied DOS of Pt NPs is significantly just below and above the Fermi level [44,45]. Hence, the small interval between the occupied and unoccupied DOS curves can lead to stronger nonlinear absorption i.e. RSA for Rh–Pt than Rh–Pd NPs as observed in Fig. 5.

The average lifetime of the excited electrons in Pd NPs has been reported to be 6 fs [46]. Thus, the electrons in the *d* band and the *s*–*p* conduction band can be sufficiently excited if the exciting laser pulse duration is longer than the lifetime regardless of the wavelength. For metal NPs with a mean diameter of nearly 10 nm, the intraband transition is strongly size dependent [3] and the contribution to SA is negative [47] or very small [48]. However, in the Rh–Pd and Rh–Pt NPs, SA was not observed. Thus, when the Rh–Pd and Rh–Pt NPs are excited by femtosecond laser pulses, the absorbed energy promotes intraband as well as interband transition between the *d* band and *s*–*p* band. Therefore, it is reasonable to consider that the intraband and interband transition between the *d* band and the *s*–*p* conduction band contribute to the RSA. Moreover, TPA has more occupied DOS in the ground state and more unoccupied DOS in excited state, then TPA takes place naturally and dominates the interband absorption when the intensity is high [5]. Further, at high intensity, the hot electrons excited by laser pulses through the intraband absorption in the conduction band and the multiphoton absorption between the *d* band and the conduction band can be further excited to a higher excited state in the conduction band, which is so-called excited state absorption (ESA) or free carrier absorption. Therefore, several phenomena such as interband transition, TPA and the participation of transient absorption of free carriers in the nonlinear absorption may surely affect the RSA.

There are two sources of nonlinear refraction, namely, electronic mechanism and thermal effect [27,46]. In this study, the thermal contribution was minimized by properly choosing the pulse duration and repetition rate of an excitation laser. The buildup time of thermal effect in aqueous solution is about 30 ns [49], which is much longer than the laser pulse duration (100 fs) used in this experiment. Besides, the repetition rate of the laser was 100 Hz, which is low enough to exclude the thermal effect. On the other hand, Hamanaka et al. proposed a model for explaining the nonlinear refraction of Ag NPs excited by femtosecond laser based on the creation of hot electrons [31]. According to this model, hot electrons are created when the excitation wavelength is far from the SPR wavelength. Hence the contribution from hot electrons due to TPA may play an important role for the Rh–Pd and Rh–Pt NPs because their SPR is far below the excitation wavelength of the employed femtosecond pulses.

4. Conclusions

In summary, a study of the third order nonlinear optical properties of the Rh–Pd and Rh–Pt alloy NPs was performed to evaluate the contribution to the nonlinear response of the addition of Pd and Pt to Rh. RSA arose from the free carriers generated by TPA. The positive nonlinear refraction of the Rh–Pd and Rh–Pt NPs was attributed to the optical Kerr effect.

Acknowledgments

The authors would like to acknowledge Dr. Yuichiro Hayasaka for his kind assistance of HAADF-STEM EDX measurements.

Disclosures

The authors declare no conflicts of interest.

References

1. U. Gurudas, E. Brooks, D. M. Bubb, S. Heiroth, T. Lippert, and A. Wokaun, "Saturable and reverse saturable absorption in silver nanodots at 532 nm using picosecond laser pulses," *J. Appl. Phys.* **104**(7), 073107 (2008).

2. R. F. Haglund, L. Yang, R. H. Magruder, J. E. Wittig, and R. A. Zuhr, "Picosecond nonlinear optical response of a Cu:silica nanocluster composite," *Opt. Lett.* **18**(5), 373–375 (1993).
3. S. Qu, Y. Zhang, H. Li, J. Qiu, and C. Zhu, "Nanosecond nonlinear absorption in Au and Ag nanoparticles precipitated glasses induced by a femtosecond laser," *Opt. Mater.* **28**(3), 259–265 (2006).
4. G. Fan, S. Qu, Q. Wang, C. Zhao, L. Zhang, and Z. Li, "Pd nanoparticles formation by femtosecond laser irradiation and the nonlinear optical properties at 532 nm using nanosecond laser pulses," *J. App. Phys.* **109**(2), 023102 (2011).
5. G. Fan, S. Ren, S. Qu, Z. Guo, Q. Wang, Y. Wang, and R. Gao, "Mechanisms for fabrications and nonlinear optical properties of Pd and Pt nanoparticles by femtosecond laser," *Opt. Commun.* **295**, 219–225 (2013).
6. R. A. Ganeev, A. I. Rysanyansky, A. L. Stepanov, and T. Usmanov, "Characterization of nonlinear optical parameters of copper- and silver-doped silica glasses at ($\lambda = 1064$ nm)," *Phys. Status Solidi B* **241**(4), 935–944 (2004).
7. N. Venkatram, D. N. Rao, and M. A. Akundi, "Nonlinear absorption scattering and optical limiting studies of CdS nanoparticles," *Opt. Express* **13**(3), 867–872 (2005).
8. V. Liberman, M. Rothschild, O. M. Bakr, and F. Stellacci, "Optical limiting with complex plasmonic nanoparticles," *J. Opt.* **12**(6), 065001 (2010).
9. N. Venkatram, R. S. S. Kumar, R. D. Narayana, S. K. Medda, S. De, and G. De, "Nonlinear optical absorption and switching properties of gold nanoparticle doped SiO₂-TiO₂ sol-gel films," *J. Nanosci. Nanotechnol.* **6**(7), 1990–1994 (2006).
10. M. Fu, K. Wang, H. Long, G. Yang, P. Lu, F. Hetsch, A. S. Susha, and A. L. Rogach, "Resonantly enhanced optical nonlinearity in hybrid semiconductor quantum dot-metal nanoparticle structures," *Appl. Phys. Lett.* **100**(6), 063117 (2012).
11. J. L. T. Chen, V. Nalla, G. Kannaiyan, V. Mamidala, W. Ji, and J. J. Vittal, "Synthesis and nonlinear optical switching of Bi₂S₃ nanorods and enhancement in the NLO response of Bi₂S₃@Au nanorod-composites," *New J. Chem.* **38**(3), 985–992 (2014).
12. D. Dini, M. J. F. Calvete, and M. Hanack, "Nonlinear optical materials for the smart filtering of optical radiation," *Chem. Rev.* **116**(22), 13043–13233 (2016).
13. H. I. Elim, J. Yang, and J. Y. Lee, "Observation of saturable and reverse-saturable absorption at longitudinal surface plasmon resonance in gold nanorods," *Appl. Phys. Lett.* **88**(8), 083107 (2006).
14. T. Cesca, P. Calvelli, G. Battaglin, P. Mazzoldi, and G. Mattei, "Local-field enhancement effect on the nonlinear optical response of gold-silver nanoplanets," *Opt. Express* **20**(4), 4537–4547 (2012).
15. J. V. Antony, P. Chandran, P. Kurian, N. P. N. Vadakkedathu, and G. E. Kochimoolayil, "Surface effects on photoluminescence and optical nonlinearity of CdS quantum dots stabilized by sulfonated polystyrene in water," *J. Phys. Chem. C* **119**(15), 8280–8289 (2015).
16. S. Porel, N. Venkatram, D. N. Rao, and T. P. Radhakrishnan, "Optical power limiting in the femtosecond regime by silver nanoparticle-embedded polymer film," *J. Appl. Phys.* **102**(3), 033107 (2007).
17. Y. Yuan, N. Yan, and P. J. Dyson, "Advances in the rational design of rhodium nanoparticle catalysts: Control via manipulation of the nanoparticle core and stabilizer," *ACS Catal.* **2**(6), 1057–1069 (2012).
18. Y. Mei, G. Sharma, Y. Lu, M. Ballauff, M. Drechsler, T. Irrgang, and R. Kempe, "High catalytic activity of platinum nanoparticles immobilized on spherical polyelectrolyte brushes," *Langmuir* **21**(26), 12229–12234 (2005).
19. S. K. Oh, Y. Niu, and R. M. Crooks, "Size-selective catalytic activity of Pd nanoparticles encapsulated within end-group functionalized dendrimers," *Langmuir* **21**(22), 10209–10213 (2005).
20. S. Alayoglu and B. Eichhorn, "Rh-Pt bimetallic catalysts: Synthesis, characterization, and catalysis of core-shell, alloy, and monometallic nanoparticles," *J. Am. Chem. Soc.* **130**(51), 17479–17486 (2008).
21. J. R. Renzas, W. Huang, Y. Zhang, M. E. Grass, and G. A. Somorjai, "Rh₁-xPd_x nanoparticle composition dependence in CO oxidation by NO," *Catal. Lett.* **141**(2), 235–241 (2011).
22. R. A. Ganeev, M. Suzuki, M. Baba, M. Ichihara, and H. Kuroda, "Low- and high-order nonlinear optical properties of Au, Pt, Pd, and Ru nanoparticles," *J. Appl. Phys.* **103**(6), 063102 (2008).
23. R. A. Ganeev, G. S. Boltaev, R. I. Tugushev, and T. Usmanov, "Nonlinear optical absorption and refraction in Ru, Pd, and Au nanoparticle suspensions," *Appl. Phys. B: Lasers Opt.* **100**(3), 571–576 (2010).
24. M. S. I. Sarker, T. Nakamura, Y. Herbani, and S. Sato, "Fabrication of Rh based solid solution bimetallic alloy nanoparticles with fully tunable composition through femtosecond laser irradiation in aqueous solution," *Appl. Phys. A* **110**(1), 145–152 (2013).
25. M. S. I. Sarker, T. Nakamura, and S. Sato, "All-proportional solid-solution Rh-Pd-Pt alloy nanoparticles by femtosecond laser irradiation of aqueous solution with surfactant," *J. Nanopart. Res.* **17**(6), 259 (2015).
26. M. S. I. Sarker, T. Nakamura, and S. Sato, "Composition-controlled ternary Rh-Pd-Pt solid-solution alloy nanoparticles by laser irradiation of mixed solution of metallic ions," *J. Mater. Res.* **29**(7), 856–864 (2014).
27. M. Sheik-Bahae, A. A. Said, T.-H. Wei, D. J. Hagan, and E. W. Van Stryland, "Sensitive measurement of optical nonlinearities using a single beam," *IEEE J. Quantum Electron.* **26**(4), 760–769 (1990).
28. R. A. Ganeev, A. I. Rysanyansky, S. R. Kamalov, M. K. Kodirov, and T. Usmanov, "Nonlinear susceptibilities, absorption coefficients and refractive indices of colloidal metals," *J. Phys. D: Appl. Phys.* **34**(11), 1602–1611 (2001).
29. X. Liu, S. Guo, H. Wang, and L. Hou, "Theoretical study on the closed-aperture Z-scan curves in the materials with nonlinear refraction and strong nonlinear absorption," *Opt. Commun.* **197**(4–6), 431–437 (2001).
30. F. Abrinaei and N. Molahasani, "Effects of Mn doping on the structural, linear, and nonlinear optical properties of ZnO nanoparticles," *J. Opt. Soc. Am. B* **35**(8), 2015–2022 (2018).

31. Y. Hamanaka, A. Nakamura, N. Hayashi, and S. Omi, "Dispersion curves of complex third-order optical susceptibilities around the surface plasmon resonance in Ag nanocrystal-glass composites," *J. Opt. Soc. Am. B* **20**(6), 1227–1232 (2003).
32. R. A. Ganeev, A. I. Rysanyansky, A. L. Stepanov, and T. Usmanov, "Saturated absorption and nonlinear refraction of silicate glasses doped with silver nanoparticles at 532 nm," *Opt. Quantum Electron.* **36**(10), 949–960 (2004).
33. S. Link and M. A. El-Sayed, "Spectral properties and relaxation dynamics of surface plasmon electronic oscillations in gold and silver nanodots and nanorods," *J. Phys. Chem. B* **103**(40), 8410–8426 (1999).
34. U. Kreibig and M. Vollmer, *Optical Properties of Metal Clusters*, (Springer, 1995).
35. N. D. Fatti and F. Vallée, "Ultrafast optical nonlinear properties of metal nanoparticles," *Appl. Phys. B: Lasers Opt.* **73**(4), 383–390 (2001).
36. D. Ricard, Ph. Roussignol, and C. Flytzanis, "Surface-mediated enhancement of optical phase conjugation in metal colloids," *Opt. Lett.* **10**(10), 511–513 (1985).
37. A. M. Watson, X. Zhang, R. Alcaraz de la Osa, J. M. Sanz, F. González, F. Moreno, G. Finkelstein, J. Liu, and H. O. Everitt, "Rhodium Nanoparticles for Ultraviolet Plasmonics," *Nano Lett.* **15**(2), 1095–1100 (2015).
38. Y. J. Xiong, J. Y. Chen, B. Wiley, Y. N. Xia, Y. D. Yin, and Z. Y. Li, "Size-dependence of surface plasmon resonance and oxidation for Pd nanocubes synthesized via a seed etching process," *Nano Lett.* **5**(7), 1237–1242 (2005).
39. C. Langhammer, Z. Yuan, I. Zorić, and B. Kasemo, "Plasmonic properties of supported Pt and Pd nanostructures," *Nano Lett.* **6**(4), 833–838 (2006).
40. R. Rosei, C. H. Culp, and J. H. Weaver, "Temperature modulation of the optical transitions involving the Fermi surface in Ag: Experimental," *Phys. Rev. B* **10**(2), 484–489 (1974).
41. J. H. Weaver, "Optical properties of Rh, Pd, Ir, and Pt," *Phys. Rev. B* **11**(4), 1416–1425 (1975).
42. N. V. Smith, "Photoemission spectra and band structures of d-band metals. III. Model band calculations on Rh, Pd, Ag, Ir, Pt, and Au," *Phys. Rev. B* **9**(4), 1365–1376 (1974).
43. O. K. Anderson, "Electronic Structure of the fcc Transition Metals Ir, Rh, Pt, and Pd," *Phys. Rev. B* **2**(4), 883–906 (1970).
44. T. Anniyev, H. Ogasawara, M. P. Ljungberg, K. T. Wikfeldt, J. B. MacNaughton, L. Naslund, U. Bergmann, S. Koh, P. Strasser, L. G. M. Pettersson, and A. Nilsson, "Complementarity between high-energy photoelectron and L-edge spectroscopy for probing the electronic structure of 5d transition metal catalysts," *Phys. Chem. Chem. Phys.* **12**(21), 5694–5700 (2010).
45. E. Puppini and P. Vavassori, "UV inverse photoemission from low-d-occupancy transition metals," *J. Phys.* **4**(25), 5551–5560 (1992).
46. M. Fierz, K. Siegmann, M. Scharfe, and M. Aeschlimann, "Time-resolved 2-photon photoionization on metallic nanoparticles," *Appl. Phys. B: Lasers Opt.* **68**(3), 415–418 (1999).
47. L. Yang, D. H. Osborne, R. F. Haglund Jr, R. H. Magruder, C. W. White, R. A. Zuhr, and H. Hosono, "Probing interface properties of nanocomposites by third-order nonlinear optics," *Appl. Phys. A* **62**(5), 403–415 (1996).
48. F. Hache, D. Ricard, C. Flytzanis, and U. Kreibig, "The optical Kerr effect in small metal particles and metal colloids: The case of gold," *Appl. Phys. A* **47**(4), 347–357 (1988).
49. Z. B. Liu, Y. Z. Zhu, Y. Zhu, S. Q. Chen, J. Y. Zheng, and J. G. Tian, "Nonlinear absorption and nonlinear refraction of self-assembled porphyrins," *J. Phys. Chem. B* **110**(31), 15140–15145 (2006).